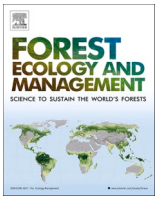
Forest Ecology and Management 598 (2025) 123231



Contents lists available at ScienceDirect

Forest Ecology and Management

journal homepage: www.elsevier.com/locate/foreco





Warmer winter-spring conditions enhance European yew radial increment more than hot-dry summers hinder it near the species southernmost distribution limit

J. Julio Camarero [a,*], Cristina Valeriano [a], Antonio Gazol [a], Miguel Ortega [a], Álvaro Rubio-Cuadrado [b,c]

[a] Instituto Pirenaico de Ecología (IPE-CSIC), Avda. Montañana 1005, Zaragoza 50059, Spain
[b] Departamento de Sistemas y Recursos Naturales, Escuela Técnica Superior de Ingeniería de Montes, Forestal y del Medio Natural, Universidad Politécnica de Madrid, Ciudad Universitaria s/n, Madrid 28040, Spain
[c] Institute of Forest Sciences (INIA, CSIC), Carretera de A Coruña km 7,5, Madrid 28040, Spain

ARTICLE INFO

Keywords:
Dendroecology
Release
Taxus baccata
Tertiary relict

ABSTRACT

The European yew (*Taxus baccata*) is a relict, protected tree species. Aridification could threaten its persistence near the xeric, southernmost distribution limit of the species. However, there are still no studies on how yew's long-term radial increment is constrained by drought, and how the drought-increment coupling interacts with land-use changes. To fill this research gap, we used dendrochronology to estimate ages and radial increment rates in six Spanish yew populations subjected to different site aridity levels. Then, climate variables and increment indices were correlated. We also reconstructed releases, which we attributed to the thinning of competing tree species. Most sampled yew trees (84 %) were recruited after the 1960s, when massive rural abandonment lead to the drastic reduction of logging and grazing in the study area. We detected releases linked to a previous thinning during the 2000s of competing pine in a dry site, and releases positively correlated with annual precipitation in the wettest site. Yew radial increment was constrained by cold winter–spring and warm–dry summer conditions (short droughts) in the driest sites. At regional level, drought–increment relationships weakened after the 1990s, when the site–to–site coherence of increment increased. Such drought–increment uncoupling and the positive increment trends observed in several yew populations, confirm that regional aridification is not negatively impacting yew performance. The decreasing influence of drought and the positive responses to warmer winter–spring conditions could be mediated by the topoclimate (shady aspect with wet–cool conditions) of the studied populations. According to radial increment data, southern yew populations inhabiting mountain climate refuges, characterized by wet–cool conditions, tolerate current aridification and their radial increment is boosted by warmer winters and springs.

1. Introduction

Climate warming and associated aridification could lead to the decline of tree populations by reducing their radial-increment rates, particularly near the species southernmost (rear edge), xeric distribution limits (Camarero et al., 2021). Tree-ring data have been widely used to assess how long-term climate conditions drive radial increment in widely distributed species (e.g., Fritts, 1976), but information on rare, relict species inhabiting topoclimatic refuges is still scarce. This is the case of the common or European yew (*Taxus baccata* L, hereafter yew), which is declining in some temperate and Mediterranean forests due to climate warming, habitat alteration and human-related disturbances such as elevated grazing pressure (Ruprecht et al., 2010; Schirone et al., 2010; Perrin and Mitchell, 2013; Kaiser et al., 2024).

Paleoecological data suggest that the current, highly fragmented yew distribution was shaped by post-glacial migration dynamics (Iszkuło et al., 2016), and in some sites, yew may have disappeared due to impacts from extreme climate events (Bebchuk et al., 2024). Massive harvest and clearance for cattle also contributed to the fragmentation and decline of yew populations (Kaiser et al., 2024). Yew is a Tertiary

* Corresponding author.
E-mail addresses: jjcamarero@ipe.csic.es (J.J. Camarero), cvaleriano@ipe.csic.es (C. Valeriano), agazol@ipe.csic.es (A. Gazol), mortegam09@gmail.co (M. Ortega), alvaro.rubio.cuadrado@upm.es (Á. Rubio-Cuadrado).

https://doi.org/10.1016/j.foreco.2025.123231
Received 8 August 2025; Received in revised form 3 October 2025; Accepted 6 October 2025
Available online 9 October 2025
0378-1127/© 2025 The Author(s). Published by Elsevier B.V. This is an open access article under the CC BY license (http://creativecommons.org/licenses/by/4.0/).

relict which experienced an ancient (ca. 6 Myr BP) separation between Eastern (Iran) and Western (Europe) populations (Mayol et al., 2015). This historical migration path explains the westward decline of genetic diversity in current yew populations and suggests that western and eastern evolutionary lineages adapted to contrasting temperature ranges and rainfall regimes (Mayol et al., 2015). Furthermore, yew often appears in mountain sites with humid, mild conditions where favorable topoclimate conditions allow it to tolerate summer water shortage near its rear edge (Linares, 2013). However, climate scenarios involving increased aridification could lead to the loss of many suitable mountain areas for yew, particularly in seasonally dry regions such as some parts of Spain (Serra, 2007). Indeed, yew radial increment is constrained by low precipitation in their eastern and southwestern European range limits, but also by cold winter-spring conditions (Cedro and Cedro, 2015; Sanchez-Martinez et al., 2020; Cedro, 2023; Kvaratskhelia and Gavashelishvili, 2025). Specifically, low summer precipitation limits yew radial increment (Sedmáková et al., 2017; Tonelli et al., 2025), but it is unknown whether yew increment is becoming more constrained by drought due to rising aridification near its rear edge. In addition, rapid forest encroachment could also contribute to yew decline because of its intermediate shade tolerance (Svenning and Magard, 1999).

Yew is a rare evergreen conifer species, usually forming small, fragmented stands, and it is considered to be long-lived with maximum lifespans of at least 500 years (Biondi, 1992; Thomas and Polwart, 2003). Yew grows in sites with diverse types of soils and light conditions, although it is more abundant on well-drained soils and mesic sites under partial shade with annual rainfall in the range of ca. 600–2000 mm (Benham et al., 2016). It is a dioecious species, which starts reproducing at ages over 70 years (Thomas and Polwart, 2003). Its fleshy fruits are mainly dispersed by birds (Hao et al., 2008). The loss of genetic diversity through inbreeding and limited gene flow among yew populations may compromise their long-term survival (Casier et al., 2024). Due to its rarity, yew is usually protected in Europe and its habitats are considered among the highest conservation priorities (Farjon, 2013; Perrin and Mitchell, 2013).

Drought has been identified as one the major constraints for yew demographic performance, including regeneration, survival and growth rates (Hulme, 1996; Sanz et al., 2009; Linares, 2013; Thomas and Garcia-Martí, 2015). Nevertheless, long-term increment data of yew are lacking, and they are particularly necessary for Mediterranean mountain sites subjected to aridification due to rising temperatures and evaporative demand. This data would allow testing how temperature and drought limit yew radial increment by simulating ring-width variability as a function of climate fluctuations using process-based models such as the Vaganov-Shashkin model (Vaganov et al., 2006). Further, interactions between land-use (e.g., forest encroachment) and climate warming during the past decades should be considered since they shaped current demographic structures of Spanish yew populations (Sanchez-Martinez et al., 2020).

The yew shares habitat and ecological conditions with very competitive tree species such as the European beech (*Fagus sylvatica* L.) (Svenning and Magard, 1999), albeit yew is often restricted to locations where the beech cannot outcompete it (rocky cliffs, peat soils, forest margins). However, the evergreen yew shows different functional traits than the deciduous beech being able to photosynthesize even in mild-oceanic winter conditions (Thomas and Polwart, 2003). Therefore, another issue regarding yew persistence is how it can be outcompeted by beech or by other widespread, fast-growing, shade-intolerant species such as Scots pine (*Pinus sylvestris* L.). This information is usually requested by managers to protect relict yew populations through thinning of more competitive tree species (Svenning and Magard, 1999; Niemczyk, 2015; Alavi et al., 2019; Ahmadi et al., 2020a, 2020b). In this sense, tree-ring data allow reconstructing growth releases which may reflect the impacts of canopy opening and reduced competition (Nowacki and Abrams, 1997).

Here, we study six yew populations in Spain, located near the species southern distribution limit, and subjected to contrasting topoclimates. We use dendrochronology to answer three questions: (i) how are the age structures and radial increment of yew?, (ii) which are the main climatic factors and drought types (severity, timing) constraining yew increment?, and (iii) can the impacts of past changes in land-use be inferred from yew age structures and ring-width data? We expect that most yews have been recruited after rural abandonment in the 1960s, when traditional land uses such as logging and grazing have ceased in many Spanish regions (Collantes and Pinilla, 2011). We also expect lower increment and drought stress in the driest sites. Finally, we hypothesize that releases will reflect past thinning to reduce competition by dominant tree species.

2. Materials and methods

2.1. Study sites and climate data

First, to assess the yew distribution in Spain we checked the ANTHOS Information System and the webpage www.anthos.es, which contains botanical information (presence) provided by the Real Jardín Botánico (CSIC). Second, we selected six study sites where at least 30 mature yew individuals were found across a ca. 1-ha area in Northern, Eastern and Central Spain (Fig. 1, Table 1).

We selected sites characterized by favorable topoclimate locations (mountains) across a wide precipitation gradient from wet-cool to dry-warm locations. Sites showed a wide elevation gradient (695 −1540 m a.s.l.). We included sites located near the xeric distribution limit of the species (e.g., sites MO and GU), which showed the highest elevation. Sites were confined to cool, shady locations with N-NW aspect (e.g., PE), and others were located on steep slopes (PN, MO). Several sites were found in mountainous areas such as the Pyrenees (LI), Iberian System (GU) or Central System (MO) and, therefore, subjected to colder conditions. In contrast, site LE was subjected to temperate wet-cool conditions, as indicated by its high aridity index and coexisting tree species (e.g., *Quercus robur*). Sites were located on limestone substrates on basic and rocky soils, excepting site MO, which was located on schist substrates and acidic soils (Serra, 2007).

To characterize the short-term climate conditions of each site (period 1993 −2022), we searched for nearby local climate stations (located less than 15 km apart) using the R package *climaemet* (Pizarro et al., 2021). Annual climate conditions and diagrams are shown in Table 1 and Fig. S1, respectively. According to these data and based on the aridity index (Zomer et al., 2022), obtained at 30 arc-seconds spatial resolution, the LE and LI sites are the wettest ones, whereas PN, GU, and MO are the driest sites showing a dry summer (Fig. S1).

The sampled sites show ongoing forest encroachment, and yew is often confined to forest margins or gaps where it shows active recruitment. For instance, many yew recruits have been found in the southernmost sites MO and GU (Balaguer Romano et al., 2020; Revilla Onrubia et al., 2021). Yew may be outcompeted by dominant tree species such as oak in site LE, European beech in site PE or Scots pine in sites LI, GU and MO (Table 1). In the site PN, yew individuals are surrounded by pine plantations of Scots pine and black pine (*Pinus nigra*), and pines outcompeting yews have been thinned or removed in the past 2 −3 decades. The understory of study sites was dominated by *Amelanchier ovalis*, *Buxus sempervirens*, *Berberis vulgaris* and *Juniperus* species.

2.2. Field sampling, climate data and drought indices

In each site, between 13 and 20 mature, apparently healthy yews were sampled. Sampling focused on dominant individuals located in relatively open areas (not suppressed, i.e. with more than 50 % of the canopy receiving direct or indirect radiation; see picture of sampled yews in Fig. 1**c**), and with a minimum diameter at 1.3 m (dbh, diameter at breast height) greater than 10 cm. Therefore, we sampled the existing range of tree sizes and ages (Tables 1 and 2). In each selected tree, we

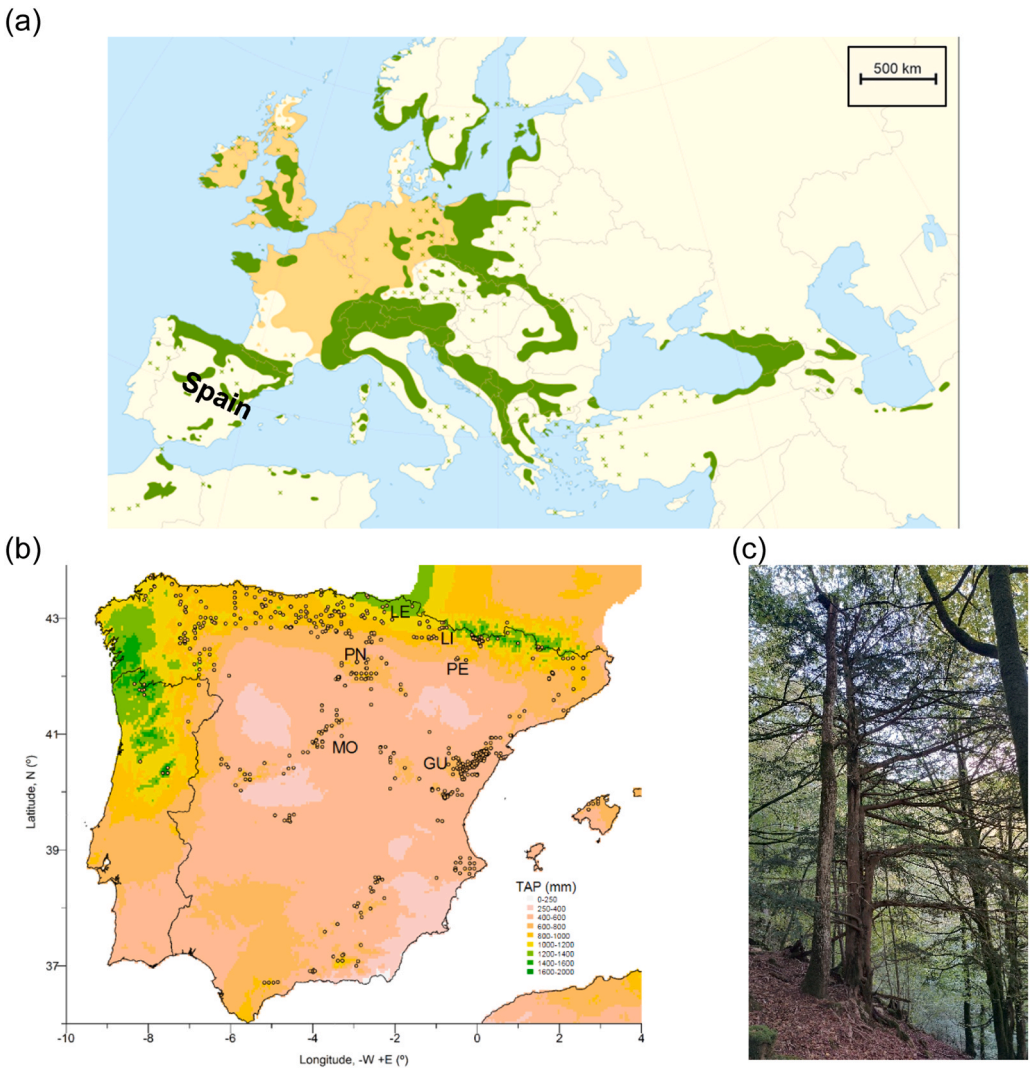


Fig. 1. (a) Distribution of yew (*Taxus baccata*) in Europe according to Caudullo et al. (2017). Green and brown patches indicate native and introduced or naturalized populations, respectively. (b) Location of the six study sites in Spain. Dots indicate yew presence according to ANTHOS data (see www.anthos.es). The background shows total annual precipitation (TAP) in the Iberian Peninsula derived from Pizarro et al. (2021). (c) View of yews sampled in site LE.

Table 1
Characteristics of the study sites. Sites are arranged in order of increasing aridity (lower values of the aridity index, AI). Diameter at breast height (dbh) values are means ± SE. Abbreviations: MAT, mean annual temperature; TAP, total annual precipitation; Ao, *Amelanchier ovalis*; Bs, *Buxus sempervirens*; Bv, *Berberis vulgaris*; Ca, *Corylus avellana*; Fe, *Fraxinus excelsior*; Fs, *Fagus sylvatica*; Ia, *Ilex aquifolium*; Js, *Juniperus sabina*; Pn, *Pinus nigra*; Ps, *Pinus sylvestris*; Qr, *Quercus robur*; Ra, *Rhamnus alpina*; Sa, *Sorbus aria*; Su, *Sorbus aucuparia*.

Site (code)	Latitude (ºN)	Longitude (°, -W, +E)	Elevation (m a.s. l.)	MAT (ºC)	TAP (mm)	AI	Slope (°)	Dbh (cm)	Other tree and shrub species
Lizara (LI)	42.763	−0.628	1432	9.8	1050	0.54	15	20.7 ± 2.1	Fs, Bs, Ia, Fe, Ao
Leitza (LE)	43.111	−1.911	695	13.6	1211	0.52	30	30.1 ± 5.4	Fs, Qr, Ia, Ca, Sa
Peiró (PE)	42.316	−0.488	1406	12.5	764	0.36	35	16.3 ± 0.5	Fs, Bs, Ao, Ps, Ia
Peñalmonte (PN)	41.191	−2.214	1144	12.4	596	0.24	47	15.7 ± 1.1	Ia, Ao, Ra, Ps, Pn
Barranco del Mosquito (MO)	41.138	−3.526	1540	11.0	676	0.22	40	19.0 ± 0.8	Ps, Ia, Su
Gúdar (GU)	40.452	−0.695	1533	11.0	653	0.21	20	11.5 ± 0.6	Ps, Bv, Ao, Ca, Js

measured its dbh and extracted two cores at the same height and perpendicular to the maximum slope using a Pressler increment borer.

To avoid problems with gaps or heterogeneous local climate data, we used the 0.1°-gridded EOBS climate dataset (v25.0e; Cornes et al., 2018). We obtained long-term, monthly data of mean maximum (TMx) and minimum (TMn) temperatures and total precipitation (Pre) for the 1950–2022 period. Seasonal (winter, previous December to current February; spring, March to May; summer, June to August; autumn, September to November) and annual predictors were obtained by averaging temperature or summing precipitation data, respectively. We also calculated the hydrological-year precipitation by summing monthly rainfall values from prior October to current September. These seasonal and annual climate predictors only refer to the current year.

To assess site aridity, we obtained the annual Aridity Index (AI) at a 30 arc-seconds (ca. 700-m) spatial resolution for the period 1970–2000 from Zomer et al. (2022). The AI is defined as the ratio between

Table 2
Characteristics of tree-ring with data considering the common period 1965 −2022. Ring-width and basal area increment (BAI) data are means ± SD. Different superscript letters indicate significantly ($p < 0.05$) different BAI values among sites according to Mann-Whitney tests.

Site (code)	No. trees	No. cores	Min. − Max. age at 1.3 m (years)	Tree-ring width (mm)	BAI ($cm^2\ yr^{-1}$)	AR1	MS	Rbar	EPS
LE	13	19	45 − 164	0.89 ± 0.64^{ab}	4.72 ± 1.54^{b}	0.84	0.30	0.38	0.88
PN	15	30	48 − 108	0.86 ± 0.57^{ab}	4.42 ± 1.66^{b}	0.69	0.43	0.62	0.98
LI	20	34	49 − 151	1.38 ± 0.34^{ab}	3.74 ± 1.02^{a}	0.71	0.42	0.36	0.85
PE	20	35	59 − 119	0.69 ± 0.40^{a}	2.02 ± 0.56^{a}	0.65	0.33	0.39	0.90
MO	21	41	30 − 60	1.81 ± 0.52^{b}	4.82 ± 3.35^{b}	0.72	0.21	0.43	0.92
GU	14	27	40 − 68	0.94 ± 0.38^{ab}	2.28 ± 0.85^{a}	0.73	0.24	0.44	0.92

precipitation to Penman-Monteith Reference Evapotranspiration (ET_0). AI values higher than 0.65 correspond to humid climates, $0.65 \geq AI > 0.50$ values are found for dry sub-humid climate conditions, and $0.50 \geq AI > 0.20$ values indicate semi-arid climates. According to these rankings, sites LE and LI can be considered to have a dry sub-humid climate, whereas sites PE, PN, MO, and GU (in order of decreasing AI) correspond to semi-arid climates (Table 1).

To assess drought severity and duration, we used monthly, 0.1°-gridded data of the Standardized Precipitation Evapotranspiration Index (SPEI) in the same period (1950–2022). The SPEI is a multi-scalar index computed from monthly rainfall, temperature and potential evapotranspiration showing cumulative water surplus or deficit (Vicente-Serrano et al., 2010). We considered 1- to 24-month-long SPEI temporal scales. We also obtained weekly SPEI data at 1- (SPEI1) and 3-month (SPEI3) long temporal scales from the 1.1-km^2 Spanish SPEI dataset (period 1965–2022; Vicente-Serrano et al., 2017) to analyze SPEI−increment relationships at finer temporal and spatial scales.

2.3. Processing tree-ring width data

Radial increment data were obtained and analyzed using dendrochronological methods including cross-dating and detrending of ring-width series (Fritts, 1976). Cores were air dried, glued onto wooden supports, and carefully sanded with progressively finer-grain sandpaper until ring boundaries were clearly visible. Then, they were scanned at 2400 dpi resolution and visually cross-dated. Ring widths were measured with a 0.01 mm resolution using scanned images and the CooRecorder-CDendro software (Larsson and Larsson, 2022). The quality of cross-dating was checked using the COFECHA software, which calculates moving correlations between individual series of ring-width values and the mean sites series (Holmes, 1983).

To assess trends in radial increment, we converted the individual ring-width series into mean basal area increment (BAI) series for each individual and site, assuming a concentric stem growth. The BAI was calculated using the following formula:

$$BAI = \pi\ (R_t^2 - R_{t-1}^2) \quad (1)$$

where R_t and R_{t-1} are the radii measured in years t and t-1, respectively, corresponding to the cumulative sums of ring widths ($\sum_i^t RW$ and $\sum_i^{t-1} RW$, respectively). Age at 1.3 m was estimated based on the oldest, cross-dated core per tree after correcting the missing innermost rings using a graphical method (Rozas, 2003).

To estimate periods of growth release, which could be linked to thinning or pruning of species competing for light with sampled yews, we calculated positive growth changes (*PGC*) following Nowacki and Abrams (1997):

$$PGC = [(M_2 - M_1) / M_1] \times 100 \quad (2)$$

where M_2 and M_1 are subsequent and previous 10-year ring-width medians calculated on individual series and shifted every year. We considered a 50 % threshold in *PGC* observed in at least 50 % of trees in each site for defining major growth changes, which were expressed as annual percentages for periods with at least 5 sampled trees. Since the annual frequencies (f) of major growth changes depend on the changing sample size (number of measured trees, n), we corrected these frequencies (f_c) following Osborn et al. (1997):

$$f_c = f \times n^{0.5} \quad (3)$$

2.4. Analyzing the climate drivers of high-frequency increment variability

To calculate climate− and SPEI−increment relationships, each tree-ring series was detrended by fitting a x-year cubic smoothing spline with a 50 % frequency response cut-off, where x was 2/3 of the mean series length. Then, we obtained ring-width indices by dividing observed by fitted values. Growth persistence in detrended ring-index series was removed by autoregressive modeling, and the pre-whitened residual series of ring-width indices were averaged using a biweight robust mean to produce residual chronologies for the six study sites. The quality of these site chronologies was assessed by calculating several dendrochronological statistics (Fritts, 1976): mean and first-order autocorrelation of ring-width data (AR1), mean sensitivity (MS) of standardized (non-prewhitened) indices, mean correlation between individual indexed series (Rbar), and the Expressed Population Signal (EPS). The series were considered to be well replicated for the period with EPS ≥ 0.85 (Wigley et al., 1984). Site chronologies were calculated using the dplR package (Bunn, 2008, 2010; Bunn et al., 2024). All analyses were carried out using the R statistical software (R Development Core Team, 2024).

2.5. Analyzing non-linear climate drivers of low-frequency increment variability

There is increasing evidence that radial-increment responses to climate are not linear (e.g., Nothdurft and Vospernik, 2018; Popa et al., 2024). Thus, we used Generalized Additive Models (GAMs; Wood, 2017) to explore non-linear climate-increment relationships focusing on low-frequency variability. GAM is a flexible semiparametric method in which the influence of predictors or covariates on the response variable is modelled with smooth functions. Thus, it allows the representation of tree radial increment trajectories and the exploration of non-linear relationships between monthly and seasonal climatic variables and tree radial increment (Wernicke et al., 2020). We proposed a series of models in which log-transformed BAI was the response variable and calendar year or yearly, monthly and seasonal climatic (maximum and minimum temperature and precipitation) were the predictors. This was done for all the studied sites, including an interaction between site (factor) and the selected predictor, and for each site separately. In all cases, the effect of the predictor was modeled with thin plate regression splines and the number of knots was set to a maximum of 5.

Separate GAMs were run for the calendar year (only when all sites are analyzed together), and for the climatic variables (maximum and minimum temperatures and precipitation) at monthly, seasonal, or yearly scales. Thus, for all sites together we run a total of 52 GAMs (year * site, and 51 climate * site models) while for each site we run 51 climate (monthly, seasonal and year) GAMs. For each model, we retained the coefficient of determination (R^2), the Akaike information criterion (AIC)

and the p value associated to the smooth of the climate variable in the case of the models for each site. To summarize the models' outputs, we plotted those variables showing a significant ($p < 0.05$) fit.

2.6. Increment simulations using the process-based Vaganov-Shashkin model

The Vaganov-Shashkin model (hereafter VS model) was employed to assess how the variability of increment indices was driven by climate fluctuations (Vaganov et al., 2006). The VS model simulates partial growth rates related to temperature (GrT) or soil moisture (GrM), which are then combined to produce an overall integral growth rate (Gr). This integral rate is a standardized sum of these partial growth rates throughout the year (Tychkov et al., 2019). The latest version of the model, VS-Oscilloscope software ver. 1.37, was employed (Shishov et al., 2016) using as input climate data (daily temperature and precipitation series from the EOBS dataset) and the site chronologies.

The VS model was parameterized for each of the six sampling sites (Table S1), with parameters tuned to maximize the Pearson correlations (r) and the synchronicity index (Gleichläufigkeit, hereafter Glk), which measures the percentage of common signs of year-to-year radial increment between the two series (Buras and Wilmking, 2015). This was done considering the calibration (1950 −1986 or 1965 −1993) and verification (1994 −2022 or 1987 −2022) periods, respectively, to account for non-stationary climate−increment relationships (Tumajer et al., 2023; Valeriano et al., 2023). All study sites share several parameters due to the species' common characteristics (Table S1), including temperature for initiation radial increment (Tbeg, excepting PN), shallow roots (LR, excepting GU), cambial cell growth rate (Vcr), and transpiration coefficient (C3).

2.7. Statistical analyses

Given the lack of normality of some variables such as BAI (assessed using Shapiro-Wilk tests), we decided to use non-parametric statistics. We used the Kendall τ to assess correlations between year and BAI or climate−increment correlations because of its accuracy with small sample sizes. To compare variables with larger sample size, such as series of BAI or major growth changes between sites, we used the Spearman correlation coefficient (r_s). To compare mean increment values between sites, Mann-Whitney tests were used.

For each site, the site chronology was used to investigate the climatic signal, considering the common period 1965–2022. Pearson correlations were calculated between the sites mean series to quantify their similarity. To test for temporal instability, 20-year moving correlations with a 1-year offset among the sites' series of ring-width indices were also calculated. In addition, a Principal Component Analysis (PCA) was calculated on the variance-covariance matrix of the site chronologies to summarize their common variability. We considered the first (PC1) and second (PC2) principal components because they accounted for more of the 75 % in the radial increment variability. The vegan package was used to calculate the PCA (Oksanen et al., 2024).

Pearson correlations were also calculated between the site chronologies and detrended monthly climatic variables (TMx, TMn and Pre), considering the window from the previous October to the current September. In the case of the SPEI, correlations were also calculated between the site chronologies and the monthly or weekly values of SPEI. Using weekly SPEI data allowed refining the timing when drought−increment correlations peaked. Lastly, 20-year moving correlations were obtained between the site chronologies or the PC1 scores and the SPEI data after selecting the SPEI temporal resolutions and months showing the highest correlations in previous analyses. Climate− and SPEI−increment correlations were calculated using the treeclim R package (Zang and Biondi, 2015).

3. Results

3.1. Increment patterns, age structure, and major growth changes

In general, increment increased as tree age decreased, whereas the highest (lowest) coherence between ring-width series was found in dry (wet) PN (LI) sites. The sites PE and MO showed the lowest and highest mean ring widths and BAI values (0.69 and 1.81 mm; 2.02 and 4.82 cm^2 yr^{-1}), respectively (Table 2). Sites PE and LE showed the lowest (0.65) and highest (0.84) AR1 values, in that order, whereas the highest MS were found in sites PN and LI (0.42 −0.43). The site MO presented the lowest MS (0.21). The highest Rbar (0.62) and EPS (0.98) values were found for site PN, and the lowest Rbar (0.36) and EPS (0.85) values corresponded to site LI.

The BAI trends differed between sites depending on tree age and site conditions. Regarding BAI values, we found two groups of slow- (sites PE and GU, 2.02 −2.28 cm^2 yr^{-1}) and fast-growing (LE, MO, and PN, 3.74 −4.82 cm^2 yr^{-1}) sites (Table 2, Fig. 2).

There was a high spatial and temporal variability in site-to-site coherence regarding BAI and ring-width data. The BAI series of sites MO and GU showed a strong and significant positive correlation ($r_s = 0.86$, $p < 0.001$), followed by the LI and MO series ($r_s = 0.57$, $p < 0.001$), whereas sites LE and GU showed a negative correlation ($r_s = -0.30$, $p = 0.02$) (Table S2). In the case of ring-width indices, the series of sites MO and GU showed positive relationships with the rest of the sites, except for site LE, and the series of site LI also showed significant positive correlations with those of sites PN and PE (Table S3). Interestingly, the site-to-site correlation of increment series was not related to the site-to-site Euclidean distance ($r_s = 0.195$, $p = 0.487$). The coherence among site series was not stable over time, increasing from the 1980s to the late 2010s, and decreasing afterwards (Fig. 2).

Most sites were dominated by young yew individuals. Most sampled yews (84 %) were recruited after the early 1960s (Fig. S2). Most trees (71 %) showed ages at 1.3 m between 40 and 75 years. The oldest yew (164 years) was sampled in site LE (Table 2), and sites LE and PE accounted for most trees older than 100 years (89 %, n = 8 trees), whereas young trees (age < 50 years) were abundant in the driest MO and GU sites which accounted for 60 % of these individuals.

There was a high spatio-temporal variability in site-to-site coherence regarding major growth changes (Fig. 3). For instance, the PN and MO series were negatively related ($r_s = -0.78$, $p < 0.001$), showing peaks in the 1970s and 2000s, and in the late 1980s, respectively. However, several sites (LE, PN, LI and PE) showed more than 25 % of their trees with major growth changes in the 1970s, which was a wet-cool decade. Interestingly, the frequency of major growth changes was positively related to 10-year shifting medians of the hydrological-year precipitation in site LE ($r_s = 0.36$, $p = 0.007$), whereas relationships were negative in the drier sites PE ($r_s = -0.38$, $p = 0.006$) and MO ($r_s = -0.73$, $p < 0.001$).

3.2. Climate−increment relationships: low-frequency variability

BAI trends depended more on temperature than on precipitation trends according to the fitted GAMs. For instance, in sites LI and GU the annual minimum temperature explained 55 % and 49 % of the BAI variability, respectively. The annual and June minimum temperatures were significant predictors of BAI in five out of the six study sites (Fig. 4). Warmer June conditions were linked to either enhanced (e.g., sites MO, GU) or reduced (e.g., sites LE, PN) BAI, and these relationships were nonlinear and significant in all sites, excepting site PE (Fig. S3).

3.3. Climate−increment relationships: high-frequency variability

Overall, yew radial increment was constrained by warm-dry spring conditions in dry sites, and by low late-winter temperatures in cool, mountain sites. High precipitation and low maximum temperatures in

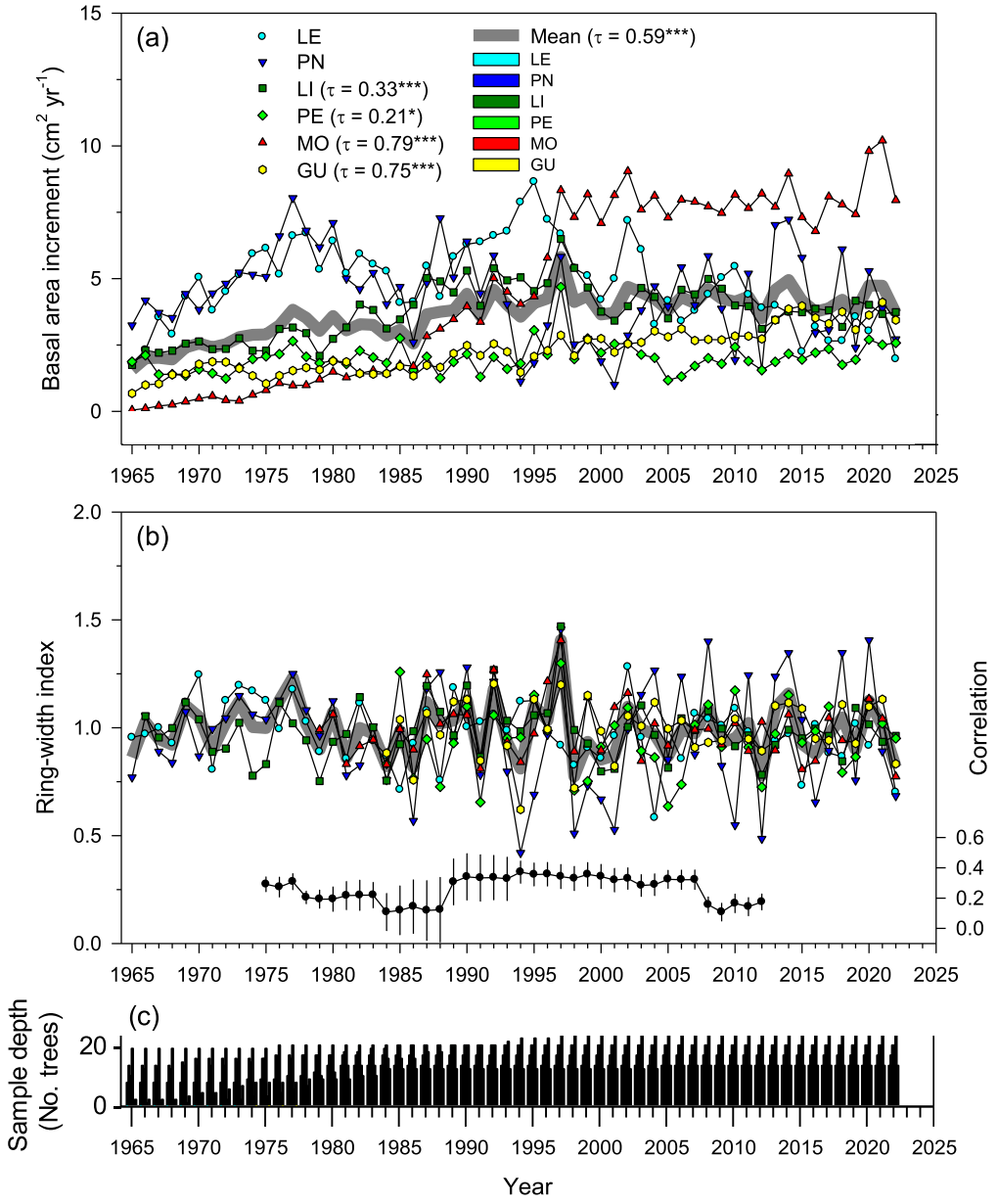


Fig. 2. Site series of (a) basal area increment (BAI), (b) ring-width indices (chronologies), and (c) sample depth (bars with same fill colors as sites' symbols in plot (a)). The dark grey lines show the respective global averages. In plot (a), the BAI trends are assessed with Kendall τ statistics during the period 1965 −2022 (*$p < 0.05$, ***$p < 0.001$). In plot (b), the right y axis shows mean 20-year moving correlations with a 1-year offset among the sites' series of ring-width indices (values are means ± SE). The dots and SE segments are located in the central year of the 20-year periods.

June-July improved yew increment in the dry PN, MO and GU sites (Fig. 5). In contrast, yew increment was constrained by low temperatures from February to March in the wetter-cooler LI and LE sites, and also by wet March-April conditions in the site LI and by warm April conditions in site LE. In site PE, increment improved in response to warmer February and April conditions. Warm April conditions also enhanced yew increment in sites PN, MO and GU.

Yew radial increment was reduced by growing-season droughts, particularly in dry sites. The correlations between the series of ring-width indices and the SPEI showed that drought constrained yew increment in the drier PN, MO and GU sites (Fig. 6). The highest correlations were found for 2-to-4-month long droughts ending from July to September. In site PE, SPEI−increment correlations peaked for 1-month December SPEI values. Lastly, no significant correlation was found in the humid site LE. The analyses with weekly SPEI values showed that increment mainly responded to 1-month SPEI values in mid-July in site MO, and to 3-month SPEI values in mid to late August in sites PN and GU (Fig. S4).

3.4. Climate-increment relationships inferred from the VS-model simulations

Year-to-year increment variability was successfully simulated by the VS-model. All simulations achieved statistically significant correlations between observed and simulated site chronologies (Table 3, Fig. S5). PE and PN sites showed low correlation values in the calibration period, possibly due to the impact of historical management or competition with other species. Additionally, the highest Glk values were found in the dry MO and GU sites indicating their sensitivity to climate variability (Table 3).

The VS-model simulations showed that yew increment peaked in spring and was constrained by dry conditions in summer. In general,

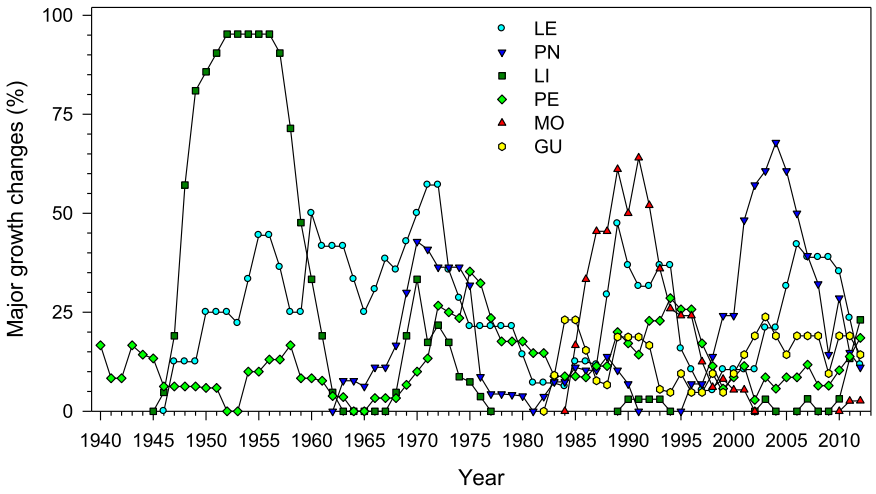


Fig. 3. Series of major growth changes calculated in the six yew study sites.

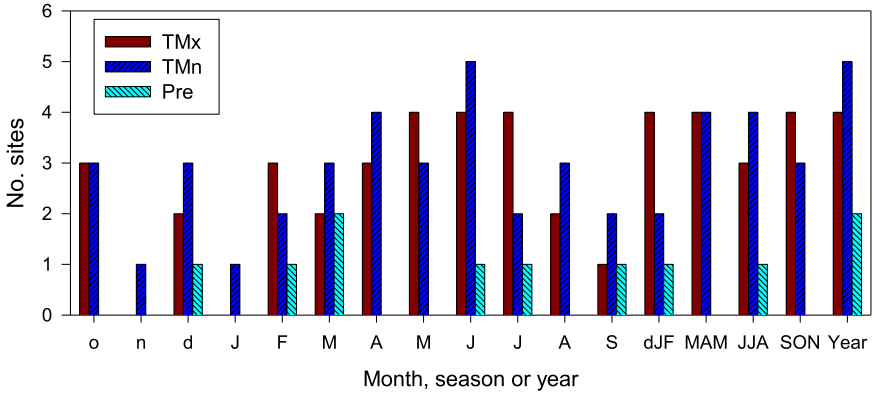


Fig. 4. Number of sites showing significant ($p < 0.05$) relationships between monthly, seasonal or annual climate variables (TMx, mean maximum temperature; TMn, mean minimum temperature; Pre, total precipitation) and BAI series according to GAMs.

yew increment peaked between late April and mid-May with a major limitation of radial increment by low soil moisture levels during late summer in the site MO, followed by sites GU and PN (Fig. 7). We also found the most constrained integral growth rates in the PN, PE, and GU sites, whereas sites LE and MO showed high growth rates (see also Table 2). There was an indication of facultative bimodal increment, with peaks in spring and autumn, in site LE. Lastly, the analyses of the changes of the main climatic constraints through time showed that MO increment was restricted by both high temperatures and low soil moisture levels in summer (Fig. S6). In other sites, radial increment was mainly limited by cold conditions (e.g., site LE) or by low soil moisture levels (e.g., site PN).

3.5. *Unstable drought-increment relationships*

The relationships between climate and radial increment were not stationary, as demonstrated the progressive uncoupling between drought and ring-width indices. During the 1965 −2022 period, the PC1 and PC2 accounted for 55.9 % and 22.6 % of the increment indices variability, respectively. Sites PN and PE showed the highest loadings along the PC1 and PC2 axes, respectively (Fig. S7). Rings with very low PC1 scores corresponded to dry years (e.g., 1986, 1994, and 2012), whereas high PC1 scores corresponded to wet years (e.g., 1997, 2013, and 2014). For instance, years 1994 and 1997 showed the lowest and highest PC1 scores, respectively, corresponding to dry (the regional July SPEI-2 was −1.13) and wet (the regional July SPEI-2 was 2.17) conditions, respectively. Consequently, the 2-month July SPEI explained 31.4 % of the temporal variability of the PC1 scores underlining the importance of drought as a major constraint of yew increment in the study sites (Fig. 8). However, the correlation between the SPEI and yew site chronologies is significantly weakening as site-to-site increment temporal variability (coefficient of variation) is increasing. The significant reduction in the strength of the correlation between SPEI and the site chronologies during the period 1980 −2022 was observed in four out of the six study sites (PE, LI, PN, and GU), with the steep decreases found in LI and PE sites, whereas it increased in the wettest LE site around 2005 (Fig. S8).

4. Discussion

Most sampled yews were relatively young with ca. 33 % showing ages between 40 and 80 years (Fig. S2). These young stands showed high radial increment values and corresponded to secondary forests established after the massive depopulation of rural Spain and the abandonment of traditional forest and woodland uses during the 1960s (Collantes and Pinilla, 2011). The low age of some dry sites such as MO explains its high increment values, whereas in older stands located in dry sites such as PE and GU, increment values were lower than in wet sites such as LE and PN. A research gap to be further explored is the impact of age and sex on how yew responds to climatic stressors (low winter temperatures, summer drought) and thinning interventions.

Our findings demonstrate that yew increment is constrained by drought stress depending on site aridity (Figs. 5 and 6). Interestingly, the radial increment of yew populations showed different responses to

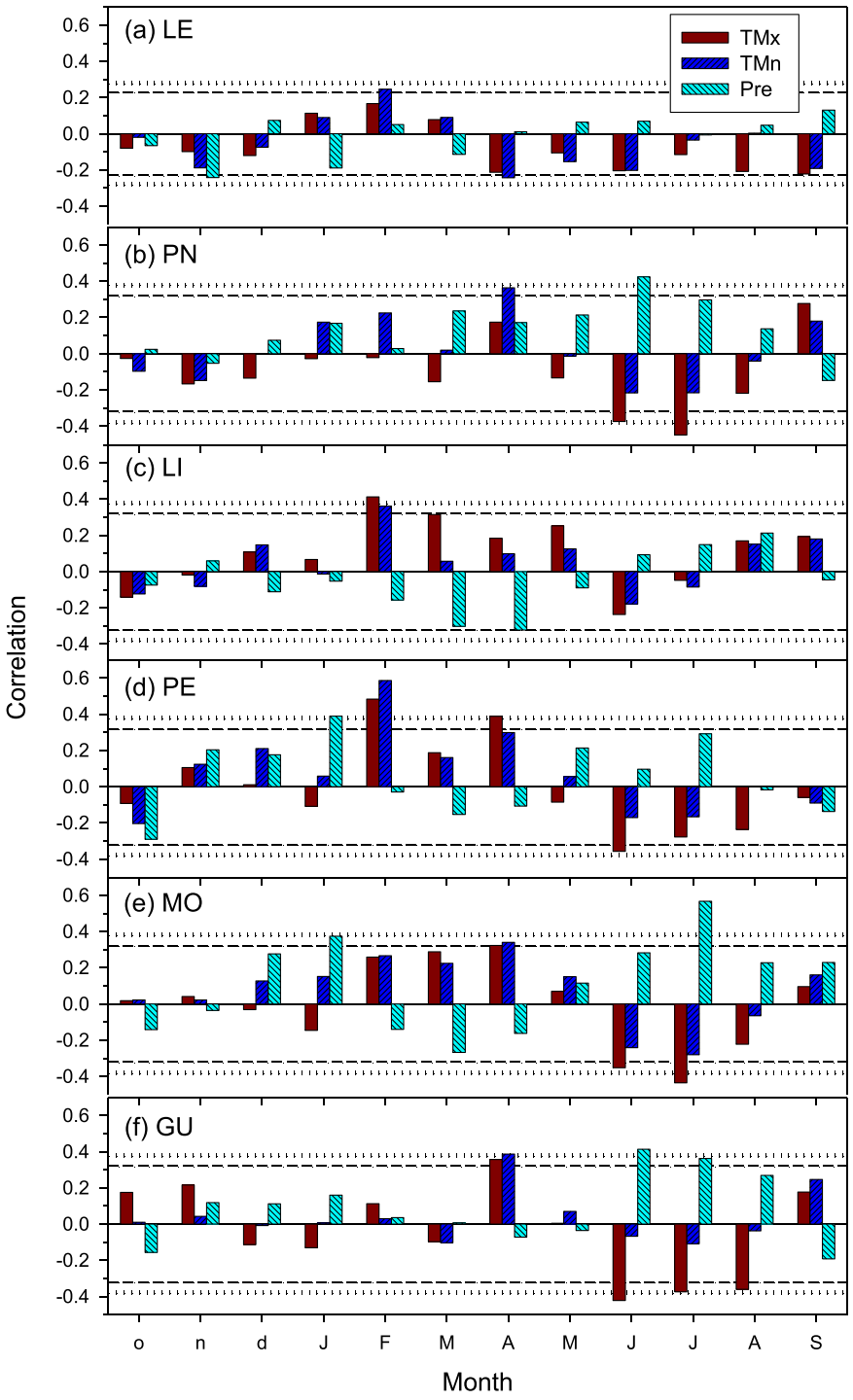


Fig. 5. Pearson correlation coefficients calculated by relating site chronologies and monthly climate variables (TMx, mean maximum temperature; TMn, mean minimum temperature; Pre, total precipitation) from the prior October to the current September. The horizontal dashed and dotted lines show the 0.05 and 0.01 significance levels, respectively. Months of the prior and current years are abbreviated by lowercase and uppercase letters, respectively.

climate when assessed at low and high-frequency variability. The BAI was more tightly related to early-summer temperature, which can be explained by a positive effect of long-term warmer conditions on yew increment, given that most study stands are located in topoclimatic refuges characterized by wet-cool conditions. However, the BAI-climate relationships assessed using GAMs could be distorted by the low age of some sites such as MO leading to highly positive responses to temperature (Fig. S3). Therefore, future studies should consider more sites and a wider range of size and age structures. In the case of the high-frequency variability, ring-width indices were more strongly correlated with winter and summer temperature and with summer precipitation confirming the yew short-term sensitive to water shortage, particularly in dry sites located near the species southernmost distribution limit (Figs. 4 and 5). Unexpectedly, the increment-drought relationship is weakening despite more arid conditions, which again emphasized the importance of local topoclimate conditions to buffer regional climate trends including aridification (Sarris and Christodoulakis, 2024; Mazza et al., 2025).

Major growth changes, detected using the Nowacki-Abrams' method, did not always reflect past thinning events because they were

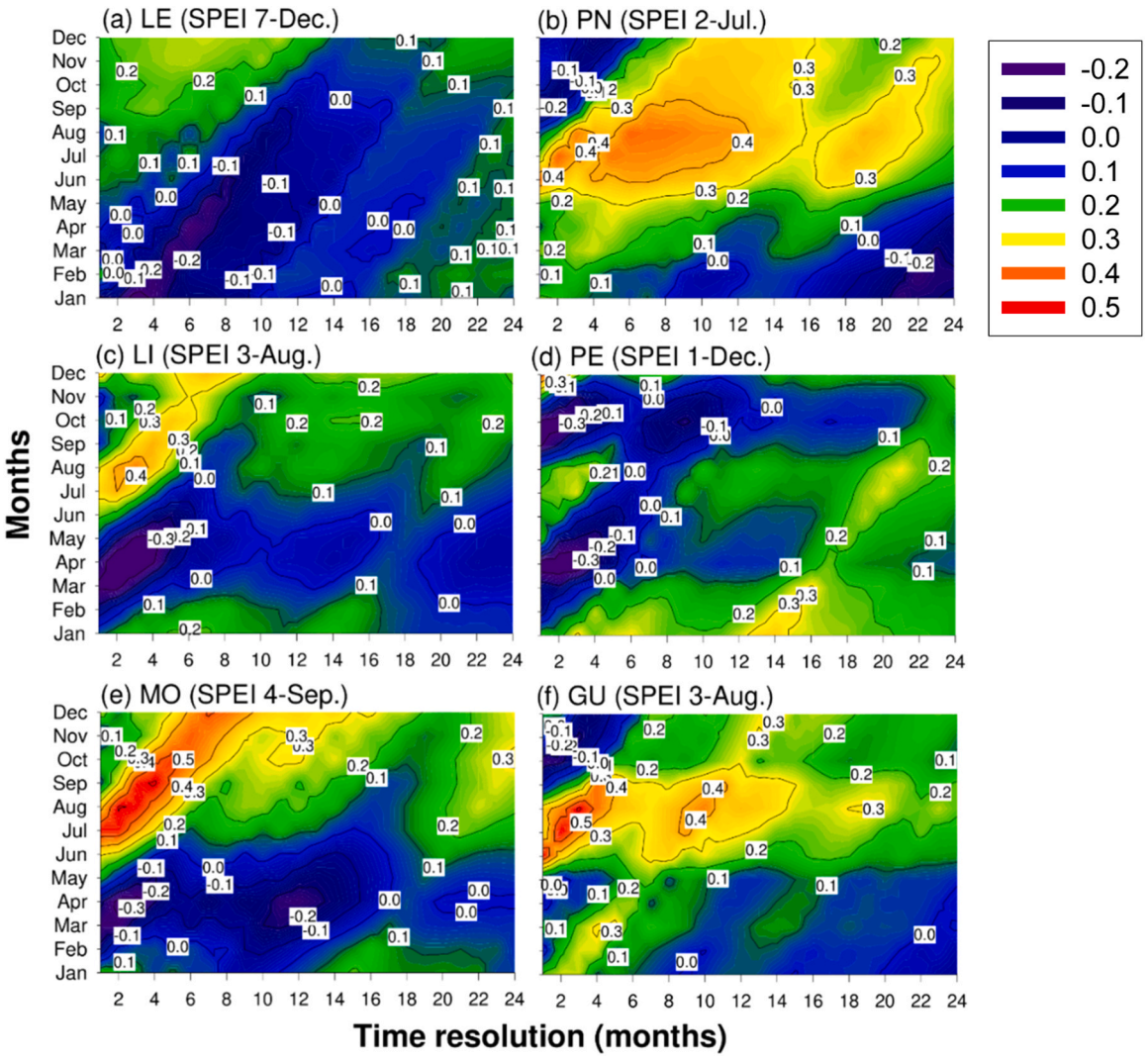


Fig. 6. Pearson correlations (color scale) calculated between site chronologies and monthly SPEI values from 1- to- 24-month long scales (x axes). After each site code, the SPEI showing the highest correlation is shown with its monthly temporal resolution and corresponding month (e.g., SPEI 4-Sep. is the 4-month September SPEI). Significant ($p < 0.05$) correlations correspond to $r \geq |0.30|$.

Table 3
Statistics of the indexed ring-width series based on the VS model and considering calibration (1950 −1986 or 1965 −1993) and verification (1994 −2022 or 1987 −2022) periods. Statistics are Pearson correlation coefficient (*r*), root-mean-square error (RMSE), and Gleichläufigkeit (Glk).

Site (code)	Period	*r*	Glk (%)	RMSE	Calibration		Verification	
					r	Glk (%)	*r*	Glk (%)
LE	1950 −2022	0.54	66	0.219	0.65	73	0.40	58
PN	1950 −2022	0.50	69	0.263	0.43	51	0.62	83
LI	1950 −2022	0.68	62	0.135	0.78	65	0.57	57
PE	1950 −2022	0.60	63	0.405	0.33	57	0.71	67
MO	1965 −2022	0.70	71	0.150	0.68	69	0.66	72
GU	1965 −2022	0.60	71	0.112	0.59	69	0.59	69

also associated with hydrological-year precipitation in the wettest LE site. However, this method detected releases in the early 2000s in the dry PN site where thinning of planted pines was carried out. There is ample evidence showing that yew is outcompeted by other tree species with faster increment rates, such as beech (*F. sylvatica*), Scots pine, silver fir (*Abies alba*) or oak species (Iszkuło et al., 2012, 2016). Regrettably, we lack historical records to confirm if releases detected in other dry sites (e.g., 1980s and 1990s in site MO) corresponded to past thinning events. Further research should compare wet and dry sites with well-dated historical records to refine the detection of growth releases in yew.

The climate− and SPEI−increment correlations and the VS-model simulations indicated different limiting factors of yew increment along the studied aridity gradient. In the wet-cool LE, LI and PE sites, radial increment was mainly constrained by low winter temperatures, whereas in the cold sites LI and PE, the impact of low late-winter temperatures on increment was more pronounced. In addition, in PE, yews are outcompeted by beech, and confined to a topoclimate refuge in N-NW slopes, where cold and shady conditions are prevalent (Villar et al., 1993). In the case of PN, yew shows increment limitations due to low

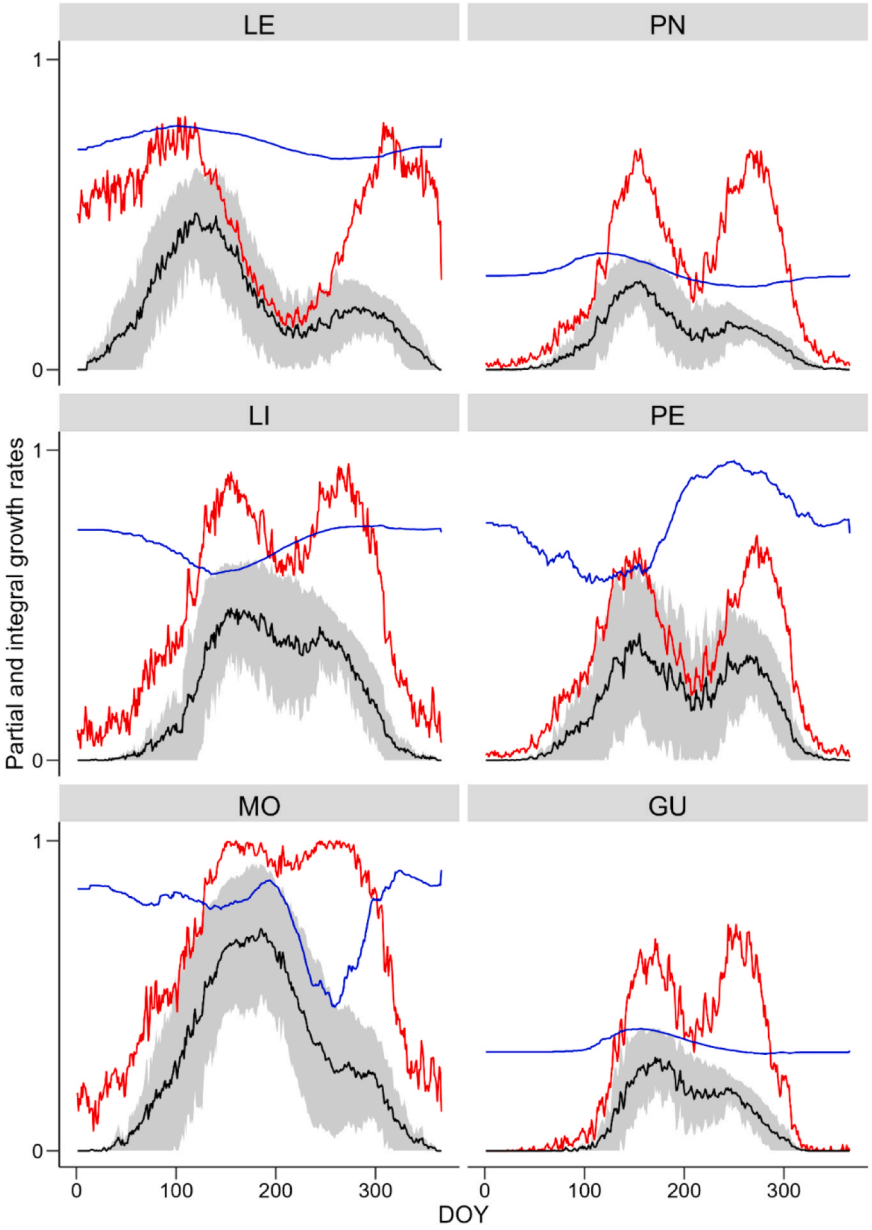


Fig. 7. Fits of the VS model showing partial growth rates (black lines) and growth rates due to temperature (red lines) or soil moisture (blue lines) limitations in the six studied yew populations.

soil moisture which could be linked to its steep slope. In addition, this yew population is surrounded by planted pines, which increase competition for light or soil water. Finally, in the dry MO and GU sites, radial increment is very limited by dry spring-summer conditions, but also by low winter temperatures. Yew wood formation is very sensitive to spring precipitation (Parsapajouh et al., 1986; Bebchuk et al., 2025; Tonelli et al., 2025). Future studies could further explore site-specific and topoclimatic conditions at the tree scale—such as soil texture and depth, slope aspect, and steepness—that influence soil moisture availability, even though preliminary findings are already available for certain conifer species (Sarris and Christodoulakis, 2024; Mazza et al., 2025).

Winter thermal conditions and summer drought were identified as key constraints of yew radial increment, which could limit the species' potential for adaptation beyond its optimal growth range in the coldest and driest sites. Previous studies on the increment responses to climate of yew evidenced its sensitivity to winter frost damage and growing-season drought in sites with a low soil water-holding capacity (Thomas and Polwart, 2003; Cedro, 2023), but also in mesic (Moir, 1999; Bebchuk et al., 2025) and cool mountain sites (Yadav and Singh, 2002). For instance, yew increment was enhanced by warm winter temperatures and wet summer conditions in Hyrcanian forests (Parsapajouh et al., 1986; Seyfullayev et al., 2021), and also near the Caspian Sea (Asadulaev et al., 2018).

We found a shift in the sensitivity of yew increment to summer drought across several of the study Spanish populations, particularly in the driest sites (Fig. 8). During the 1990s, site-to-site increment similarity and temporal increment variability both increased, whereas the drought–increment correlation weakened. This uncoupling cannot be explained by regional climate trends because aridification is being amplified by warmer conditions and higher evaporative demand across the Mediterranean Basin (Seager et al., 2014). We suggest two possible explanations. First, warmer winter-spring conditions could boost yew increment more than the detrimental effects of warmer and drier summer conditions due to favorable topoclimate conditions in shady, cool slopes. Second, warmer conditions could benefit more yew than other

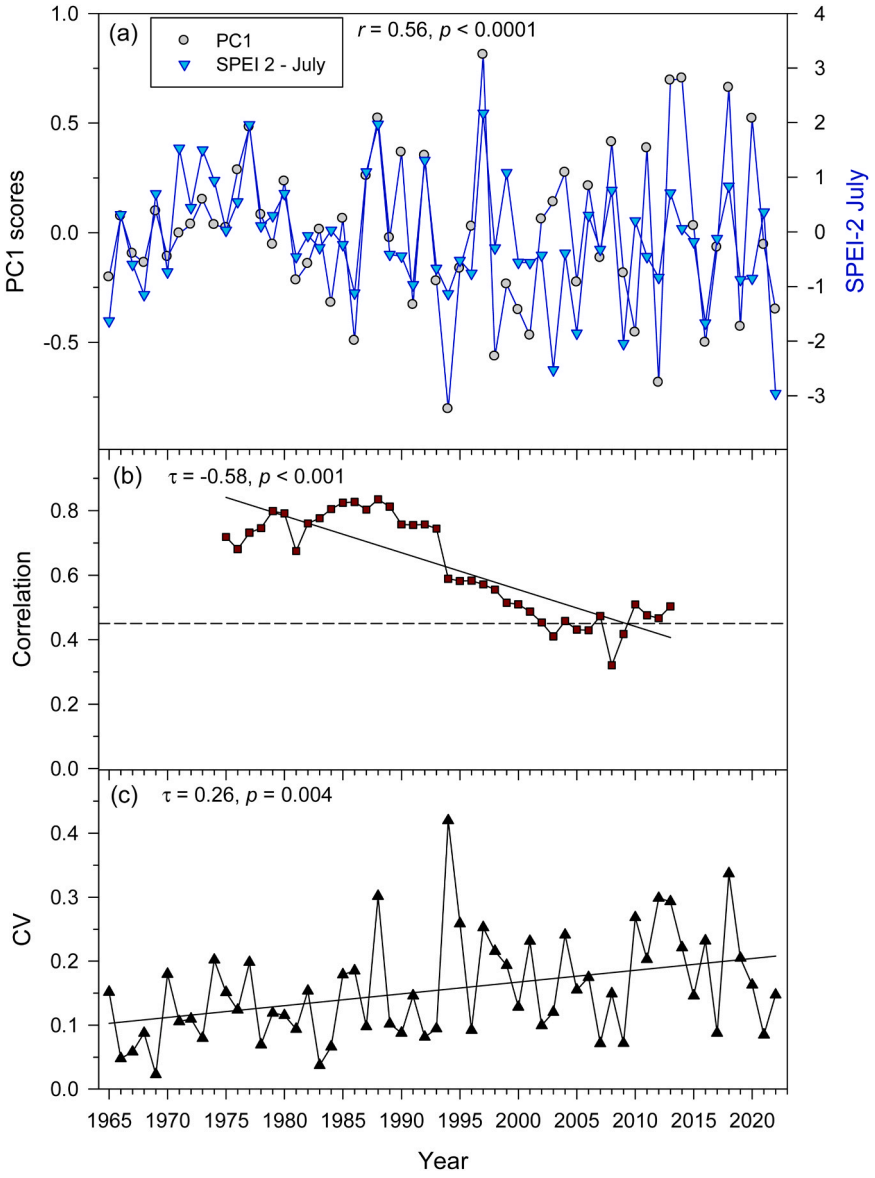


Fig. 8. (a) The PC1 scores of the site chronologies are strongly and positively related to wet summer conditions (SPEI-2 July, blue line, right *y*-axes), (b) but this correlation is weakening through time (20-year moving correlations between PC1 scores and the SPEI), and (c) the site-to-site increment is increasing through time (CV, coefficient of variation, lower plot). In plots (b) and (c), trends were quantified using the Kendall τ statistic. The dashed horizontal line in plot (b) shows the 0.05 significance level for correlation coefficients.

species (e.g., beech) and reduce competition for soil water and nutrients. However, data on stand structure would be needed to refute this hypothesis. Nevertheless, most sampled yews were growing in relatively open areas where competition with other species is probably low. Testing these ideas would require comparing tree-ring series with other proxies such as wood isotope and density data, and characterizing stand structure and dynamics. In addition, the geographical extent of the drought−increment uncoupling should be explored in other European countries.

5. Conclusions

Warmer winter-spring conditions are enhancing European yew radial increment more than hot-dry summers are constraining it near the species southernmost distribution limit. The positive effect of rising temperatures on rear-edge yew stands can be understood considering their topoclimate mountain refuges. This may explain why yew increment is uncoupling from drought stress and being enhanced by warmer conditions. Such positive effect could be complemented by selective thinning of competing tree species (beech, pine) to further enhance yew performance and to expand yew populations. Thinning could also contribute to create mixed and heterogeneous yew stands, encompassing different climatic niches, which may be more resilient to climate change.

Forecasted more arid conditions could constrain yew increment in the driest sites leading to habitat loss of the species, limiting yew shifts in the species distribution or altering sex ratios impairing reproductive performance of marginal populations restricted to wet topoclimate refuges. The implications of our research include long-term monitoring of the ecological requirements of southernmost sensitive yew populations, integrated with genetic research to improve their conservation. Lastly, our conclusions would also strengthen by sampling wider biogeographical gradients encompassing more sites under cooler and drier conditions and explicitly considering tree features (diameter, age and sex) to model yew long-term increment. Further research should clarify the adaptive potential of southernmost yew populations inhabiting dry

sites, supporting their conservation through thinning of competing tree species and by planting more resilient provenances better suited to increasing aridification.

CRediT authorship contribution statement

Antonio Gazol: Writing – review & editing, Visualization, Validation, Software, Resources, Methodology, Investigation, Funding acquisition, Data curation. **Miguel Ortega:** Writing – review & editing, Resources, Methodology, Investigation, Data curation. **Alvaro Rubio-Cuadrado:** Writing – review & editing, Supervision, Resources, Methodology, Investigation, Formal analysis, Data curation, Conceptualization. **J. Julio Camarero:** Writing – original draft, Visualization, Validation, Software, Resources, Project administration, Methodology, Investigation, Funding acquisition, Formal analysis, Data curation, Conceptualization. **Cristina Valeriano:** Writing – review & editing, Visualization, Software, Methodology, Investigation, Formal analysis, Data curation.

Declaration of Competing Interest

Authors declare no competing interests.

Acknowledgements

We thank several Spanish institutions for providing sampling permissions, including the Environment and Agriculture Departments of La Rioja, Madrid, Navarra and Aragón regional Governments. This work was supported by projects PID2021–123675OB-C43 and TED2021–129770B-C21 (Spanish Ministry of Science and Innovation). We also thank Amandine Asal and Irene Turienzo for performing preliminary tree-ring analyses.

Appendix A. Supporting information

Supplementary data associated with this article can be found in the online version at doi:10.1016/j.foreco.2025.123231.

Data availability

Data will be made available on request.

References

Ahmadi, K., Alavi, S.J., Amiri, G.Z., Hosseini, S.M., Serra-Diaz, J.M., Svenning, J.C., 2020a. The potential impact of future climate on the distribution of european yew (*taxus baccata* L.) in the hyrcanian forest region (Iran). Int. J. Biometeorol. 649, 1451–1462. https://doi.org/10.1007/S00484-020-01922-Z.

Ahmadi, K., Jalil Alavi, S., Amiri, G.Z., Hosseini, S.M., Serra-Diaz, J.M., Svenning, J.C., 2020b. Patterns of density and structure of natural populations of *taxus baccata* in the hyrcanian forests of Iran. Nord. J. Bot. 38 njb02598.

Alavi, S.J., Ahmadi, K., Hosseini, S.M., Tabari, M., Nouri, Z., 2019. The response of English yew (*taxus baccata* L.) to climate change in the caspian hyrcanian mixed forest ecoregion. Reg. Environ. Change 19, 1495–1506.

Asadulaev, Z.M., Omarova, O.K., Ramazanova, Z.K., 2018. Age and climatic bases of the variability of annual growth rings of *taxus baccata* in foothill dagestan. For. Eng. J. 8, 22–36.

Balaguer Romano, R., Sainz Ollero, H., Vasco Encuentra, F., 2020. Yew (*taxus baccata* L.) population dynamics in the iberian Mediterranean mountains: natural regeneration and expansion in east central system (Spain). For. Syst. 29, eSC03.

Bebchuk, T., Krusic, P.J., Pike, J.H., Piermattei, A., Friedrich, R., Wacker, L., Crivellaro, A., Arosio, T., Kirdyanov, A.V., Gibbard, P., Brown, D., Esper, J., Reinig, F., Büntgen, U., 2024. Sudden disappearance of yew (*taxus baccata*) woodlands from eastern england coincides with a possible climate event around 4.2 ka ago. Quat. Sci. Rev. 323, 108414.

Bebchuk, T., Moir, A.K., Arosio, T., Kirdyanov, A.V., Torbenson, M.C.A., Krusic, P.J., Hindson, T.R., Howard, H., Buchwal, A., Norman, C.A.P., Büntgen, U., 2025. Taxus tree-ring chronologies from Southern england reveal Western european hydroclimate changes over the past three centuries. Clim. Dyn. 63, 108. https://doi.org/10.1007/s00382-025-07601-2.

Benham, S.E., Houston Durrant, T., Caudullo, G., de Rigo, D., 2016. *taxus baccata* in Europe: distribution, habitat, usage and threats. In: San-Miguel-Ayanz, J., de Rigo, D., Caudullo, G., Houston Durrant, T., Mauri, A. (Eds.), In: European Atlas of Forest Tree Species. Publications Office of the EU, Luxembourg.

Biondi, F., 1992. Development of a tree-ring network for the Italian peninsula. TreeRing Bull. 52, 15–29.

Bunn, A.G., 2008. A dendrochronology program library in r (dplR). Dendrochronologia 26, 115–124. https://doi.org/10.1016/j.dendro.2008.01.002.

Bunn, A.G., 2010. Statistical and visual crossdating in r using the dplr library. Dendrochronologia 28, 251–258. https://doi.org/10.1016/j.dendro.2009.12.001.

Bunn, A.G., Korpela, M., Biondi, F., Campelo, F., Mérian, P., Qeadan, F., Zang, C., 2024. dplR: Dendrochronology Program Library in R. R package version 1.7.7, ⟨https://CRAN.R-project.org/package=dplR⟩.

Buras, A., Wilmking, M., 2015. Correcting the calculation of Gleichläufigkeit. Dendrochronologia 34, 29–30. https://doi.org/10.1016/J.DENDRO.2015.03.003.

Camarero, J.J., Gazol, A., Sangüesa-Barreda, G., Vergarechea, M., Alfaro-Sánchez, R., Cattaneo, N., Vicente-Serrano, S.M., 2021. Tree growth is more limited by drought in rear-edge forests most of The Times. For. Ecosyst. 8, 25.

Casier, M., Van Diest, A., Aerts, R., Peeters, G., Van Acker, K., Hellemans, B., Honnay, O., Muys, B., 2024. Genetic diversity and structure of endangered native yew *taxus baccata* in remnant populations in Belgium. For. Ecol. Manag. 553, 121633. https://doi.org/10.1016/j.foreco.2023.121633.

Caudullo, G., Welk, E., San-Miguel-Ayanz, J., 2017. Chorological maps for the main european woody species. Data Brief. 12, 662–666. https://doi.org/10.1016/j.dib.2017.05.007.

Cedro, A., 2023. Dendrochronology and dendroclimatology of yew in Poland. Dendrochronologia 78, 126068.

Cedro, A., Cedro, B., 2015. Growth-climate relationships at yew and wild service trees on the eastern edge of their range in Europe. For. Syst. 24, e044.

Collantes, F., Pinilla, V., 2011. Peaceful Surrender: The Depopulation of Rural Spain in the Twentieth Century. Cambridge Scholars Publishing, Cambridge, UK.

Cornes, R.C., van der Schrier, G., van den Besselaar, E.J.M., Jones, P.D., 2018. An ensemble version of the E-OBS temperature and precipitation data sets. J. Geophys. Res. Atm. 123, 9391–9409.

Farjon, A., 2013. Taxus baccata. IUCN Red. List Threat. Species 2013. https://doi.org/10.2305/IUCN.UK.2013-1.RLTS.T42546A2986660.en. Accessed 13 June 2024.

Fritts, H.C., 1976. Tree Rings and Climate. Academic Press, London.

Hao, D.C., Xiao, P.G., Huang, B.L., Ge, G.B., Yang, L., 2008. Interspecific relationships and origins of taxaceae and cephalotaxaceae revealed by partitioned Bayesian analyses of chloroplast and nuclear DNA sequences. Plant Syst. Evol. 276, 89–104.

Holmes, R.L., 1983. Program COFECHA user's manual. Laboratory of Tree–Ring Research, The University of Arizona, Tucson, USA.

Hulme, P.E., 1996. Natural regeneration of yew (*taxus baccata* L.): microsite, seed or herbivore limitation? J. Ecol. 1, 853–861.

Iszkuło, G., Didukh, Y., Giertych, M.J., Jasińska, A.K., Sobierajska, K., Szmyt, J., 2012. Weak competitive ability May explain decline of *taxus baccata*. Ann. For. Sci. 69, 705–712. https://doi.org/10.1007/s13595-012-0193-4.

Iszkuło, G., Pers-Kamczyc, E., Nalepka, D., Rabska, M., Walas, L., Dering, M., 2016. Postglacial migration dynamics helps to explain current scattered distribution of *taxus baccata*. Dendrobiology 76, 81–89.

Kaiser, K., Theuerkauf, M., van der Maaten, E., et al., 2024. Forest history from a single tree species perspective: natural occurrence, near extinction and reintroduction of european yew (*taxus baccata* L.) on the Darss-Zingst peninsula, Southern baltic sea coast. Eur. J. For. Res. 143, 917–942. https://doi.org/10.1007/s10342-024-01665-1.

Kvaratskhelia, R., Gavashelishvili, A., 2025. Common yew (*taxus baccata*) as a climate archive: reconstructing 200 years of temperature change in Georgia (Caucasus). Dendrochronologia 89, 126285. https://doi.org/10.1016/j.dendro.2024.126285.

Larsson, L.A., Larsson, P.O., 2022. CDendro and CooRecorder. Cybis Elektron. Data AB Saltsjöbaden Swed. v. 9.8.1.

Linares, J.C., 2013. Shifting limiting factors for population dynamics and conservation status of the endangered English yew (*taxus baccata* L., Taxaceae). For. Ecol. Manag. 291, 119–127. https://doi.org/10.1016/j.foreco.2012.11.009.

Mayol, M., Riba, M., González-Martínez, S.C., Bagnoli, F., de Beaulieu, J.L., Berganzo, E., Burgarella, C., Dubreuil, M., Krajmerová, D., Paule, L., Romšáková, I., Vettori, C., Vincenot, L., Vendramin, G.G., 2015. Adapting through glacial cycles: insights from a long-lived tree (*taxus baccata*). New Phytol. 208, 973–986. https://doi.org/10.1111/nph.13496.

Mazza, G., Manetti, M.C., Kraushaar, G., Pezzi, G., Krebs, P., Coşgun, S., Tinner, W., Conedera, M., 2025. Climate sensitivity of *abies alba* mill. In marginal Mediterranean low-elevation stands reveals new insights into the ecological potential of the species. For. Ecol. Manag. 585, 122670. https://doi.org/10.1016/j.foreco.2025.122670.).

Moir, A.K., 1999. The dendrochronological potential of modern yew (*taxus baccata*) with special reference to yew from hampton court palace, UK. New Phytol. 144, 479–488.

Niemczyk, M., 2015. The influence of stand canopy openness on the growth of common yew (*taxus baccata* L.). For. Res. Pap. 76, 42–48.

Nothdurft, A., Vospernik, S., 2018. Climate-sensitive radial increment model of Norway spruce in tyrol based on a distributed lag model with penalized splines for year-ring time series. Can. J. For. Res. 48, 930–941.

Nowacki, G.J., Abrams, M.D., 1997. Radial-growth averaging criteria for reconstructing disturbance histories from pre-settlement-origin oaks. Ecol. Monogr. 67, 225–249.

Oksanen, J., Simpson, G., Blanchet, F., Kindt, R., Legendre, P., et al., 2024. vegan: Community Ecology Package. R package version 2.6-5, ⟨https://github.com/vegandevs/vegan⟩.

Osborn, T.J., Briffa, K.R., Jones, P.D., 1997. Adjusting variance for sample-size in tree-ring chronologies and other regional mean timeseries. Dendrochronologia 15, 89–99.

Parsapajouh, D., Bräker, O.U., Habibi, H., Schär, E., 1986. Étude dendroclimatologique du bois de *taxus baccata* du nord de l'Iran. Schweiz. Z. fur Forstwes. 137, 853–868.
Perrin, P.M., Mitchell, F.J.G., 2013. Effects of shade on growth, biomass allocation and leaf morphology in european yew (*taxus baccata* L.). Eur. J. For. Res. 132, 211–218. https://doi.org/10.1007/s10342-012-0668-8.
Pizarro, M., Hernangómez, D., Fernández-Avilés, G., 2021. climaemet: Climate AEMET Tools. doi:10.5281/zenodo.5205573, ⟨https://hdl.handle.net/10261/250390⟩.
Popa, A., Popa, I., Badea, O., Bosela, M., 2024. Non-linear response of Norway spruce to climate variation along elevational and age gradients in the Carpathians. Environ. Res. 252, 119073.
R Development Core Team. 2024. R: A Language and Environment for Statistical Computing. Vienna, Austria.
Revilla Onrubia, A., Vasco, F., Thomsen, A., Braschi, J., Bernal, R., Fernández, P., Murillo, J.A., Génova, M., 2021. El censo como herramienta para conocer y proteger la tejeda del mosquito (DOI). Conserv. óN. Veg. 25, 19–22. https://doi.org/10.15366/cv2021.25.004.
Rozas, V., 2003. Tree age estimates in *fagus sylvatica* and *quercus robur*: testing previous and improved methods. Plant Ecol. 167, 193–212.
Ruprecht, H., Dhar, A., Aigner, B., Oitzinger, G., Klumpp, R., Vacik, H., 2010. Structural diversity of English yew (*taxus baccata* L.) populations. Eur. J. For. Res. 129, 189–198. https://doi.org/10.1007/s10342-009-0312-4.
Sanchez-Martinez, P., Marcer, A., Mayol, M., Riba, M., 2020. Shaping the niche of *taxus baccata*, a modelling exercise using biologically meaningful information. For. Ecol. Manag. 501, 119688.
Sanz, R., Pulido, F., Nogués-Bravo, D., 2009. Predicting mechanisms across scales: amplified effects of abiotic constraints on the recruitment of yew *taxus baccata*. Ecography 32, 993–1000.
Sarris, D., Christodoulakis, D., 2024. Topographic and climatic effects on *pinus halepensis* s.l. Growth at its drought tolerance margins under climatic change. J. Res 35, 102. https://doi.org/10.1007/s11676-024-01755-1.
Schirone, B., Ferreira, R.C., Vessella, F., Chirone, A., Piredda, R., Simeone, M.C., 2010. *taxus baccata* in the azores: a relict form at risk of imminent extinction. Biodivers. Conserv 19, 1547–1565. https://doi.org/10.1007/s10531-010-9786-0.
Seager, R., Liu, H., Henderson, N., Simpson, I., Kelley, C., Shaw, T., Ting, M., 2014. Causes of increasing aridification of the Mediterranean region in response to rising greenhouse gases. J. Clim. 27, 4655–4676.
Sedmáková, D., Saniga, M., Kucbel, S., Pittner, J., Kỳpetová, M., Jaloviar, P., Bugala, M., Vencurik, J., Lukácik, I., 2017. Irregular shelterwood cuttings promote viability of european yew population growing in a managed forest: a case study from the Starohorské mountains, Slovakia. Forests 8. https://doi.org/10.3390/f8080289.
Serra, L. (ed.), 2007. El Tejo en el Mediterráneo Occidental. Generalitat Valenciana, Alicante, Spain.
Seyfullayev, F., George, S.T., Farzaliyev, V., Thapa, U.K., Guillet, S., Stoffel, M., 2021. The dendroclimatological potential of common yew (*taxus baccata* L.) from Southern Azerbaijan. TreeRing Res 77, 32–37. https://doi.org/10.3959/TRR2020-6.
Shishov, V.V., Tychkov, I.I., Popkova, M.I., Ilyin, V.A., Bryukhanova, M.V., Kirdyanov, A. V., 2016. VS-oscilloscope: a new tool to parameterize tree radial growth based on climate conditions. Dendrochronologia 39, 42–50. https://doi.org/10.1016/j.dendro.2015.10.001.
Svenning, J.C., Magard, E., 1999. Population ecology and conservation status of the last natural population of English yew (*taxus baccata*) in Denmark. Biol. Conserv 88, 173–182. https://doi.org/10.1016/S0006-3207(98)00106-2.
Thomas, P.A., Garcia-Martí, X., 2015. Response of european yews to climate change: a review. For. Syst. 24, eR01. https://doi.org/10.5424/fs/2015243-07465.
Thomas, P.A., Polwart, A., 2003. Biological flora of the British isles: *taxus baccata* l. J. Ecol. 91, 489–524.
Tonelli, E., Avanzi, C., Bitocchi, E., Vitali, A., Piotti, A., Spanu, I., Barocci, E., Urbinati, C., 2025. Variation in radial growth sensitivity to drought among genetic groups of common yew (*taxus baccata* L.) in central Italy. Dendrochronologia 92, 126360.
Tumajer, J., Begovic, K., Cada, V., Jenicek, M., Lange, J., Masek, J., Kaczka, R.J., Rydval, M., Svoboda, M., Vlcek, L., Treml, V., 2023. Ecological and methodological drivers of non-stationarity in tree growth response to climate. Glob. Chang. Biol. 29, 462–476. https://doi.org/10.1111/gcb.16470.
Tychkov, I.I., Sviderskaya, I.V., Babushkina, E.A., Popkova, M.I., Vaganov, E.A., Shishov, V.V., 2019. How can the parameterization of a process-based model help us understand real tree-ring growth? Trees Struct. Funct. 33, 345–357. https://doi.org/10.1007/s00468-018-1780-2.
Vaganov, E.A., Hughes, M.K., Shashkin, A.V., 2006. Growth dynamics of tree rings: Images of past and future environments. Springer, Berlin, New York.
Valeriano, C., Tumajer, T., Gazol, A., González de Andrés, E., Sánchez-Salguero, R., Colangelo, M., Linares, J.C., Valor, T., Sangüesa-Barreda, G., Camarero, J.J., 2023. Delineating vulnerability to drought using a process-based growth model in pyrenean silver fir forests. For. Ecol. Manag. 541, 121069.
Vicente-Serrano, S.M., Beguería, S., López-Moreno, J.I., 2010. A multiscalar drought index sensitive to global warming: the standardized precipitation evapotranspiration index. J. Clim. 23, 1696–1718. https://doi.org/10.1175/2009JCLI2909.1.
Vicente-Serrano, S.M., Tomas-Burguera, M., Beguería, S., Reig, F., Latorre, B., et al., 2017. A high resolution dataset of drought indices for Spain. Data 2, 22. https://doi.org/10.3390/data2030022.
Villar, L., Romo, A.M., Perdigo, M.T., 1993. The beechwoods of the central Pre-Pyrenees (Spain). a preliminary survey for conservation. Biol. Conserv 66, 85–93.
Wernicke, J., Körner, M., Möller, R., Seltmann, C.T., Jetschke, G., Martens, S., 2020. The potential of generalized additive modelling for the prediction of radial growth of Norway spruce from central Germany. Dendrochronologia 63, 125743.
Wigley, T.M.L., Briffa, K.R., Jones, P.D., 1984. On the average value of correlated time series, with applications in dendroclimatology and hydrometeorology. J. Clim. Appl. Meteor. 23, 201–213.
Wood, S.N., 2017. Generalized additive models: an introduction with R. Chapman and Hall/CRC.
Yadav, R.R., Singh, J., 2002. Tree-Ring analysis of *taxus baccata* from the Western himalaya, India, and its dendroclimatic potential. Tree Ring Res 58, 23–29.
Zang, C., Biondi, F., 2015. Treeclim: an r package for the numerical calibration of proxy-climate relationships. Ecography 38, 431–436.
Zomer, R.J., Xu, J., Trabucco, A., 2022. Version 3 of the global aridity index and potential evapotranspiration database. Sci. Data 9, 409. https://doi.org/10.1038/s41597-022-01493-1.